Polydimethylsiloxane (PDMS) composites for optical ultrasound generation and multi-modality imaging

Sacha Noimark[a,b,c*], Richard J. Colchester[a,b*], Radhika K. Poduval[d], Efthymios Maneas[a,b], Erwin J. Alles[a,b], Tianrui Zhao[c], Edward Z. Zhang[a,b], Michael Ashworth[e], Elena Tsolaki[b], Adrian H. Chester[f], Najma Latif[f], Sergio Bertazzo[b], Anna L. David[a,g], Sebastien Ourselin[a,b], Paul C. Beard[a,b], Ivan P. Parkin[a,c], Ioannis Papakonstantinou[d] and Adrien E. Desjardins[a,b]

[a] Wellcome-EPSRC Centre for Interventional and Surgical Sciences, University College London, UK
[b] Department of Medical Physics and Biomedical Engineering, University College London, Gower Street, London WC1E 6BT, UK
[c] Materials Chemistry Research Centre, Department of Chemistry, University College London, 20 Gordon Street, London WC1H 0AJ, UK
[d] Department of Electronic and Electrical Engineering, University College London, Gower Street, London, WC1E 6BT, UK
[e] Histopathology Department, Camelia Botnar Laboratories, Great Ormond Street Hospital for Children NHS Trust, Great Ormond Street, London, WC1N 3JH, UK
[f] National Heart and Lung Institute, Heart Science Centre, Imperial College London, Middlesex, UB9 6JH, UK
[g] Institute for Women's Health, University College London, 86-96 Chenies Mews, London, WC1E 6HX, United Kingdom

* Authors contributed equally

Abstract

Polydimethylsiloxane (PDMS) is widely used in biomedical science and can be manipulated to form composites that have broad applicability. One promising application where PDMS composites offer several advantages is optical ultrasound generation via the photoacoustic effect. Here, we review and classify methods to create these PDMS composites. We highlight how the composites can be applied to a range of substrates, from micron-scale, temperature-sensitive optical fibres to centimetre-scale curved and planar surfaces. The resulting composites have enabled all-optical ultrasound imaging of biological tissues both *ex vivo* and *in vivo*, with high spatial resolution and with clinically-relevant contrast. In addition to this review, we present the first three-dimensional all-optical pulse-echo ultrasound imaging of *ex vivo* human tissue, using a PDMS-multi-walled carbon nanotube composite and a fibre-optic ultrasound receiver. We also present gold nanoparticle-PDMS and crystal violet-PDMS composites with prominent absorption at one wavelength range for pulse-

echo ultrasound imaging, and transmission at a second wavelength range for photoacoustic imaging. We obtained images of diseased human vascular tissue with both structural and molecular contrast. With a broader perspective, we highlight literature on recent advances in PDMS micro-fabrication from different fields and suggest methods for incorporating them into new generations of optical ultrasound generators.

1 Introduction

Polydimethylsiloxane (PDMS) is an elastomeric polymer that has found broad applicability in biomedical sciences, including strain sensing[1–3], microfluidics[4,5], energy harvesting[6,7], and photomechanical actuators[8]. It can be shaped and patterned with features ranging from macroscopic to nanoscopic scales[9]. Additionally, many techniques have been developed to alter its optical, thermal, and electrical properties to make it attractive for a wide range of applications[10–14].

PDMS has recently shown great promise in the development of composite coatings for optical ultrasound generation[15–21]. Here, pulsed or modulated excitation light is absorbed within an engineered material, which results in transient heating and a corresponding pressure rise via the photoacoustic effect[22]. The resulting propagating ultrasound waves can have a high peak-to-peak pressure and a large bandwidth (i.e. a wide range of ultrasound frequencies), which lead to large imaging depths and high spatial resolution, respectively. One attractive feature of optical ultrasound generation is the potential to fabricate highly miniaturised fibre-optic components with scalable processes. These components can be integrated into medical devices such as catheters and needles to provide real-time image guidance[23]. Fibre-optic ultrasound transmitters have the additional advantages of being immune to electromagnetic interference and MRI-compatible. Collectively, these properties make optical ultrasound generation well suited for clinical diagnostic and therapeutic applications, such as guidance of minimally-invasive surgical procedures.

Several material properties of PDMS composites are important for optical ultrasound generation (Table 1). For a given coating, the generated ultrasound pressure (p) is proportional to the coating's optical absorption coefficient (μ_a) and its Grüneisen parameter (Γ)[22,24]: $p \propto \mu_a \Gamma$. The Grüneisen parameter can be defined by the coating properties as $\Gamma = \beta c_s^2 / C_p$, where β is the volume thermal expansion coefficient, c_s is the speed of sound, and C_p is the specific heat capacity at constant pressure[22,24]. One of the beneficial properties of PDMS is its large volume thermal expansion

coefficient[25] ($\beta \sim$ 300 x 10^{-6} C^{-1}), which leads to a higher value of Γ. However, in its native form, PDMS has a low optical absorption coefficient in the wavelength range of 400 to 1100 nm[26]. To achieve higher values of μ_a, optical absorbers can can be integrated into PDMS. Several optical absorbers have been integrated for different applications[2,4,10–12]. However, this integration process is not always straightforward, as the hydrophobicity of the pre-cured PDMS limits the type of absorbers that can be integrated, and it can be challenging to achieve homogeneous composites. Moreover, maintaining small coating thicknesses to reduce acoustic attenuation[27,28] and maintain wide bandwidths for high resolution imaging can be difficult. These difficulties can be particularly acute for coatings deposited on highly miniaturised, temperature-sensitive or non-uniform substrates. Different coating strategies have been used to minimise coating thicknesses whilst maintaining high optical absorption.

For efficient ultrasound generation, thermal and stress confinement conditions must be met[22,29], which can result in restrictions on the thickness of the composites. According to these conditions, the temporal width of the optical excitation pulse, τ_p, must be shorter than the time periods of both thermal conduction, τ_{th}, and stress propagation, τ_s, across the optically absorbing region in the composite[29]. Both conditions depend on the characteristic length of the absorbing region (L_p), defined as the penetration depth of incident light, or the thickness of the absorbing region (whichever is shortest). The thermal conduction time depends on the geometry of the structure[30], but it can be approximated as $\tau_{th} \sim L_p^2/4D_T$, where D_T is the thermal diffusivity of the composite[29]. Similarly, the stress propagation time can be estimated as $\tau_s \sim L_p/c_s$[29]. To maximise thermal conduction and stress propagation times, the speed of sound and thermal diffusivity can be minimised. For native PDMS, the thermal diffusivity and speed of sound are *ca.* 1.1 x 10^{-7} m^2s^{-1} and *ca.* 1080 ms^{-1}, respectively[31,32], but they can vary with the addition of optical absorbers[10,27]. Alternatively, increasing the characteristic length of the absorbing region will also increase thermal conduction and stress propagation times. However, a shorter characteristic length of the absorbing

region is required to achieve wider bandwidths. This can be achieved by reducing the composite thickness or by increasing the optical absorption coefficient. If the coating thickness is reduced and the optical absorption coefficient is unchanged, less light will be absorbed and therefore the generated ultrasound pressure will be reduced. Likewise, if the optical absorption coefficient is increased but the coating thickness is unchanged, the light will be absorbed over a smaller region and therefore the temperature increase will be larger. This larger temperature increase can lead to thermal damage of the coating. In addition, when the characteristic length of the absorbing region is too short, the thermal confinement condition is not met. Thus, in practice, there is often a trade-off between maximising ultrasound pressure and ultrasound bandwidth.

Physical Attribute		**Advantage**
Small coating thickness	=	Reduced acoustic attenuation; wide ultrasound bandwidth[27,28] (5 – 100 MHz for imaging)
High thermal expansion coefficient (β)[25]	=	High optical to ultrasound conversion efficiency[22] for high pressure (0.5 – 5 MPa at a few MPa)
High optical absorption (μ_a)	=	High pressure
Strong adhesion to glass	=	High damage threshold for high pressure[16]
Biocompatibility	=	Ease of medical translation
Refractive index similar to glass substrates[33,34]	=	High coupling of excitation light into the coating
Acoustic impedance similar to biological tissue[35,36]	=	Efficient coupling of ultrasound into tissue

Table 1: Desired coating properties for optimal optical ultrasound generation which lead to increased depths and resolution in imaging applications.

In this article, we review materials for ultrasound generation and highlight the use of PDMS as a host material for optical absorbers. We examine fabrication processes used to create PDMS composites with high optical absorption, and discuss their advantages for optical ultrasound generation. These fabrication processes involve different PDMS deposition techniques such as spin-coating, electrospinning and dip-coating, to minimise coating thicknesses and maximise ultrasound bandwidths. We categorise PDMS composites for optical ultrasound generation according to their fabrication method, as follows: (i) “all-in-one” methods, in which the PDMS and optically absorbing component are mixed prior to coating the substrate to achieve heterogeneous composites; (ii)

"bottom-up" methods, in which the optically absorbing material is coated on the substrate and subsequently over-coated with optically transparent PDMS to achieve a bilayer composite; (iii) "top-down" methods in which optically transparent PDMS is applied to the substrate and the optical absorber is subsequently incorporated to achieve a micron-scale composite region (Figure 1). In addition to a review of literature on bottom-up fabrication methods, we present the first 3D all-optical ultrasound image of *ex vivo* human tissue using optical ultrasound transmitters, highlighting the potential for clinical applications. The use of a top-down PDMS composite coating method can broaden the capabilities of these ultrasound transmitters, as we demonstrated with two novel composites for dual-modality imaging with all-optical pulse-echo ultrasound and photoacoustic imaging.

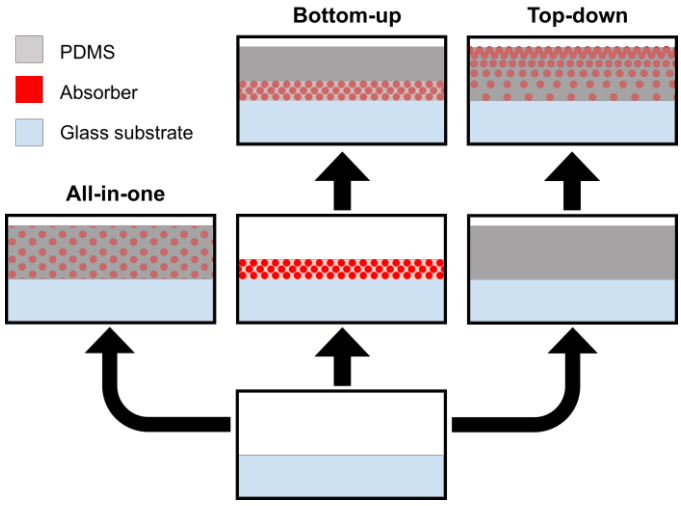

Figure 1. Three coating methods for fabricating PDMS composites for optical ultrasound generation.

2 Coating Strategies for Optical Ultrasound Generation

The use of PDMS as a host material for the optically absorbing component has shown great promise for improving properties of materials for optical ultrasound generation compared to simple metallic films[37]. These absorber-host composites show increased generated ultrasound pressures and damage thresholds compared to absorber-only coatings[16]. Several optically absorbing materials have been considered for integration with PDMS, which include carbonaceous materials such as carbon black (CB)[38,39] and multi-walled carbon nanotubes (MWCNTs)[15,16,37], as well as metallic

nanoparticles[17,37] (Table 2). The following three sections will discuss how these coatings, comprising different spatial distributions of optical absorbers, have been fabricated using all-in-one, bottom-up, and top-down methods.

Author	Optically absorbing material	Coated substrate	Measured distance (mm)	Measured pressure (MPa)	-6 dB bandwidth (MHz)	Laser fluence (mJ/cm^2)
Baac *et al*.[15]	MWCNT	Concave lens	5.5	32	~20	42.4
Baac *et al*.[37]	AuNP MWCNT	Glass slide	-	-	~80 ~80	3 mW/cm^2*
Lee *et al*.[40]	MWCNT	Concave lens	9.2	70	25	9.6
Colchester *et al*. [19]	MWCNT	105 µm core optical fibre 200 µm core optical fibre	2	0.45 0.9	12 15	41.6 36.3
Noimark *et al*.[20]	MWCNT	200 um core optical fibre	3	1.34 – 4.5	23.15 – 39.8	16.2 – 87.9
Chang *et al*.[39]	CSNP CNF CB Cr	Glass slide	4.2	4.8 2.3 0.8 0.4	~21 ~10 ~12 ~13	3.57
Wu *et al*.[41]	AuNP	Glass slide	1.8	0.01 – 0.189	~4	3.67 – 13
Zou *et al*.[17]	AuNP	400 um core optical fibre	1	0.64	~8	8.75
Hou *et al*.[42]	AuNP	Glass slide	10	0.002	~65	20.4
Buma *et al*.[38]	CB	Glass slide	10	0.150	-	10.4
Poduval *et al*.[43]	MWCNT	200 µm core optical fibre	1.5	0.2 – 1.59	29	35
Hsieh *et al*.[44]	CNF CB	Glass slide	3.65	12.15 1.60	7.63 7.84	3.71
Lee and Guo[45]	Cr Ti	Planar glass	-	~0.6 – 1.82 ~0.5 – 1.0	-	2.35

Table 2: Ultrasound characteristics of optical ultrasound generators using PDMS composite. AuNP = gold nanoparticles, MWCNT = multi-walled carbon nanotubes, CSNP = candle soot nanoparticles, CNF = carbon nanofibers, CB = carbon black, Cr = chromium, Ti = titanium. The tilde symbol '~' indicates that values presented here were estimated from a graph in the corresponding publication. The asterisk symbol '*' indicates that there was insufficient information to calculate the fluence.

2.1 All-in-one Fabrication

All-in-one fabrication methods, in which a pre-formed PDMS-composite is deposited onto a desired substrate, can be used to fabricate both metallic nanoparticle- and carbonaceous-PDMS composite coatings. One example of a metallic nanoparticle-based composite has been developed by Zou *et al*.[17]. Here they synthesised a gold nanoparticle (AuNP) and PDMS composite by mixing gold salt

with the PDMS precursors (Sylgard-184)[17]. The AuNPs (*ca.* 20 nm) were formed by the *in-situ* reduction of gold, and the concentration of AuNPs could be tuned by varying the initial amount of gold salt added. The AuNP-PDMS composite solution was applied to the distal end of optical fibres with dip-coating, thereby forming a domed coating that was 105 µm at its maximum thickness. Upon excitation with 532 nm pulsed light, the coated fibres achieved ultrasound pressures of 0.64 MPa at a distance of 1 mm from the coating surface and were used to acquire a speed of sound image through a slice of pork tissue[17]. Zou *et al.* highlighted the difficulty in controlling the coating thickness using this method[17]. The authors suggested the use of focused ion beam milling to help achieve fine control of the nanocomposite film thickness[17] and thereby to increase the bandwidth.

Colchester *et al*.[19] and Noimark *et al*.[20] used solution-based methods for achieving carbonaceous composite films on optical fibres with micron-scale thickness. MWCNTs were functionalised using an oleylamine-functionalised pyrene ligand to facilitate their dissolution in solvents compatible with PDMS such as xylene or toluene[19]. This MWCNT formulation was directly mixed with medical grade PDMS to reduce its viscosity. The MWCNT-PDMS composite solution was applied onto optical fibres by dip-coating methods, which resulted in domed coatings that were less than 20 µm at their thickest point[19]. The MWCNT-PDMS optical ultrasound transmitters fabricated by Colchester *et al*. achieved peak ultrasound pressures of 0.89 MPa at a distance of 2 mm from the coating surface, with a corresponding bandwidth of 15 MHz. Through optimisation of the MWCNT formulation and fabrication steps, Noimark *et al*. created thinner coatings, which lead to peak-to-peak ultrasound pressures in excess of 3 MPa at 3 mm and corresponding bandwidths of 30 MHz[20]. Optical ultrasound transmitters fabricated using these types of coatings were used for pulse-echo ultrasound imaging of *ex vivo* swine aorta and carotid artery samples, and achieved an axial resolution superior to 60 µm[46] (Figure 2). In addition, Alles *et al*. demonstrated that with the use of an adaptive light modulation technique, imaging could be achieved with these types of probes using a compact diode laser[47].

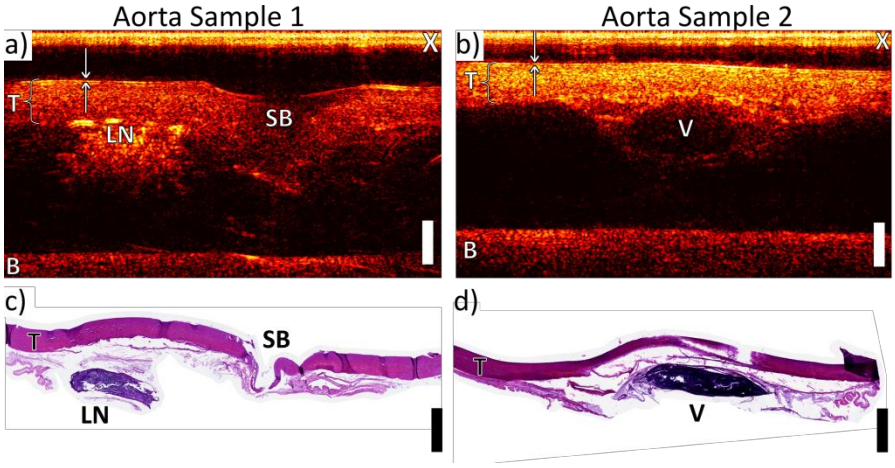

Figure 2. (a) and (b) are all-optical ultrasound images of swine aorta with tunica media (T), cross-talk (X), the base of the tissue mount (B), a side branch (SB), a lymph node (LN) and a vessel (V), labelled. Arrows indicate two reflective layers which may correspond to the intima boundaries. Also shown in (c) and (d) are histology of aorta sections corresponding to images (a) and (b), respectively. Scale bar: 2 mm. Adapted with permission.[46] Copyright 2015, The Optical Society.

The all-in-one fabrication method can be used to coat both miniature optical fibre targets and large planar surfaces. Using spin-coating methods, Buma *et al*. created CB-PDMS composite coatings on a glass substrate for optical ultrasound transmission[48]. They compared the performance of the CB-PDMS composites to thin chromium film optical ultrasound transmitters, which are commonly used as a reference for the optical ultrasound generation performance of new materials[37,39,48]. The use of toluene in the CB-PDMS polymer solution may have contributed to the small coating thicknesses that were achieved (*ca.* 25 µm). These CB-PDMS composite coatings on glass substrates were 16 times more efficient at optical ultrasound generation than a 0.15 µm thick chromium film without PDMS[48]. However, they exhibited very high increases in acoustic attenuation with ultrasound frequency (nearly 1 dB/µm at 100 MHz)[28]. To further minimise coating thickness, the viscosity of the composite solution was decreased further by improving the CB dispersion. This improvement was achieved by the use of larger CB particle sizes, and by removing the solvent component from the composite solution as it was found to inhibit CB dispersion[49]. The resulting spin-coated films

had a thickness of 11 μm and a light-to-ultrasound conversion efficiency 3.5 times higher than that of previous thicker CB-PDMS composite coatings[49]. These results highlight the importance of minimising film thicknesses to maximise ultrasound generation efficiency.

Fabrication of ultrasound transmitter materials using all-in-one methods presents several advantages. For instance, the prepared formulation comprising PDMS and integrated optical absorbers can be applied onto substrates of varying sizes and morphologies. One limitation that may arise with all-in-one methods is the challenge presented by optimisation of the composite and its deposition for ultrasound generation. Additionally, this method can lead to the inefficient use of expensive nanomaterials that are incorporated into polymers with short working times.

2.2 Bottom-up Fabrication

Bottom-up fabrication methods can exploit many coating-deposition techniques that have been developed to deposit thin absorbing coatings directly onto glass substrates, prior to over-coating with PDMS. By minimising the thickness of the ultrasound generating coating, the resulting ultrasound bandwidth and pressure can be improved (Table 1). Such coatings can comprise carbonaceous optical absorbers[15,16,37,39,44] and metallic nanoparticles[37,42]. A PDMS over-coat can be applied to these thin absorbing coatings using spin-coating or dip-coating techniques.

Thin absorbing films using metallic nanoparticles can be formed on glass substrates using focused ion beam or lithography methods[42,50–52]. One example is the optical ultrasound transmitter by Hou *et al*., which was fabricated using nanoimprint lithography and spin-coating to create an AuNP array and a PDMS over-coat, respectively[42]. The transmitted ultrasound pressures were estimated as 1.5 MPa at the coating surface, with corresponding broad bandwidths (*ca.* 65 MHz). Exploiting the wavelength-selective nature of the AuNP array, this research was subsequently extended to devices that could be used as both ultrasound receivers and ultrasound transmitters. These devices were

fabricated using the AuNP array and a gold mirror deposited on top of the PDMS layer to form an optical cavity[51]. Imaging of a metal wire phantom demonstrated high axial and lateral resolutions of 19 µm and 38 µm, respectively[51]. The authors proposed, as extensions of their research, translation of this coating technology onto optical fibre bundles as a step towards real-time imaging, and optimisation of the nanostructures to maximise optical absorption[51].

Metallic films can be inefficient optical ultrasound generators due to two limitations: their low thermal expansion coefficients and their high optical reflectivities. To overcome the first limitation, Lee and Guo fabricated optical ultrasound transmission structures comprising a metallic film sandwiched between two thermally-expansive polymer layers[45]. Ultrathin metallic films (chromium, titanium) were deposited using sputtering techniques and the polymer coatings were applied using spin-coating (PDMS) or physical vapour deposition (parylene). Polymer/metal/polymer sandwich structures deposited on glass substrates outperformed coatings comprising metallic films over-coated with a polymer. In all cases, structures using PDMS polymer layers outperformed those comprising parylene. The improved ultrasound performance of the PDMS sandwich structures, as compared to those with parylene, were attributed to the high thermal expansion coefficient of PDMS. To address the second limitation, an aluminium film over-coat was applied to create a resonant optical cavity to increase the optical absorption of the structure. Using a system comprising a PDMS/chromium/PDMS/aluminium layered structure, transmitted ultrasound pressures of up to 1.82 MPa were achieved.

Bottom-up fabrication methods have also been used to create carbonaceous PDMS composites on glass substrates for broadband optical absorption. These carbonaceous materials include MWCNTs[15,16,20,37], candle soot nanoparticles (CSNPs)[39], and carbon nanofibers (CNFs)[44] deposited using methods as diverse as electrospinning, dip-coating and chemical vapour deposition (CVD). Electrospinning methods have been used to create two different PDMS composites for optical

ultrasound generation. Firstly, Hsieh *et al*. used electrospinning to deposit a polyacrylonitrile mesh onto a glass slide and subsequently carbonised it at 900°C in a nitrogen atmosphere, to create an absorbing CNF film (Figure 3 (a))[44]. A PDMS over-coat was applied using spin-coating, which resulted in a CNF-PDMS composite coating on a planar glass substrate for optical ultrasound generation[44]. The ultrasound transmitter generated an ultrasound pressure of 12.15 MPa at a distance of 3.65 mm from the coating. This is more than sufficient for ultrasound imaging applications where highly miniaturising the lateral dimensions of the transmitter is not critical. Poduval *et al*. used electrospinning methods to create MWCNT-PDMS composite coatings for optical ultrasound generation[43]. In this study, the coatings were formed directly onto optical fibres, which resulted in highly miniaturised ultrasound transmitters that are potentially well-suited for minimally invasive surgical applications[43]. To create these coatings, the MWCNTs were functionalised using cetyl trimethylammonium bromide (CTAB) for dispersion in water and then mixed with polyvinyl alcohol (PVA) to form a MWCNT-PVA electrospinning solution. Electrospinning methods resulted in a mesh-like coating of PVA fibres with incorporated MWCNTs, which was directly formed onto the optical fibre tip and subsequently over-coated with PDMS by dip-coating (Figure 3 (b)-(d))[43]. Directly electrospinning the MWCNTs onto the optical fibre presented several advantages such as MWCNT alignment within the PVA fibres for enhanced optical absorption, and precise control over the coating thicknesses. The resulting optical ultrasound transmitters generated ultrasound pressures of up to 1.59 MPa, as measured at 1.5 mm from the coatings. Whilst the ultrasound pressures are lower than those generated by the planar CNF-PDMS ultrasound transmitters fabricated by Hsieh *et al*., the significantly smaller source diameters of the optical fibre-based transmitters will lead to greater ultrasound divergence, which could potentially increase the lateral image resolution.

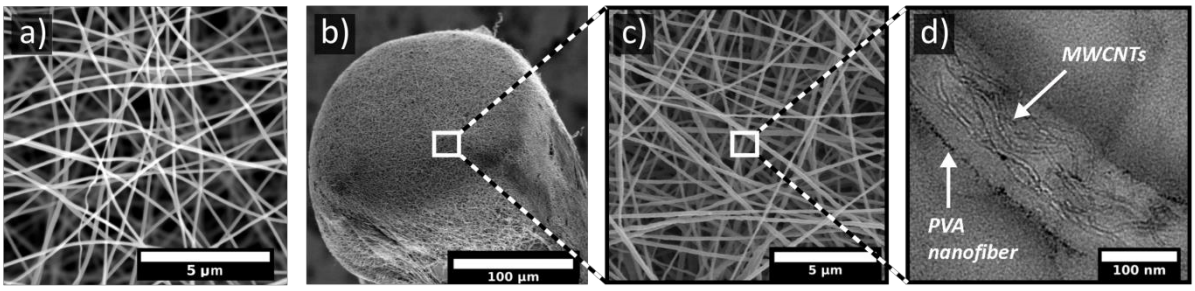

Figure 3. SEM images of (a) electrospun carbon nanofibre film. Adapted with permission.[44] Copyright 2015, AIP Publishing LLC. (b) electrospun PVA-MWCNT nanofibre coating on an optical fibre tip, (c) high magnification image of PVA-MWCNT mesh. (d) TEM image of MWCNTs encapsulated in a PVA nanofibre. (b)-(d) Adapted under the terms of the CC-BY-4 license.[43] Copyright 2017, Poduval *et al*.

Chang *et al*. developed a novel method of fabricating highly absorbing carbon-PDMS composites using candle soot nanoparticles (CSNPs)[39]. These were deposited on a glass microscope slide by positioning it above a candle flame, and a PDMS over-coat was subsequently applied using spin-coating[39]. The ultrasound performance of the CSNP-PDMS coatings was compared to a series of PDMS composites including a CB-PDMS composite (all-in-one fabrication), a CNF-PDMS composite (as prepared by Hsieh *et al.*[44]), and a chromium-PDMS composite (bottom-up fabrication). The CSNP-PDMS composite outperformed the other composites in terms of generated ultrasound pressure: *ca*. 2 times greater than CNF-PDMS, 6 times greater than CB-PDMS, and 16 times greater than chromium-PDMS. Moreover, the ultrasound bandwidth of the CSNP-PDMS composite was broader (*c.f.* Table 2). In this study, the superior performance of the CSNP-PDMS composite compared to other tested carbonaceous-PDMS composites may have been due to the large surface-to-volume ratio, which provided more rapid heat dissipation to the surrounding PDMS[39].

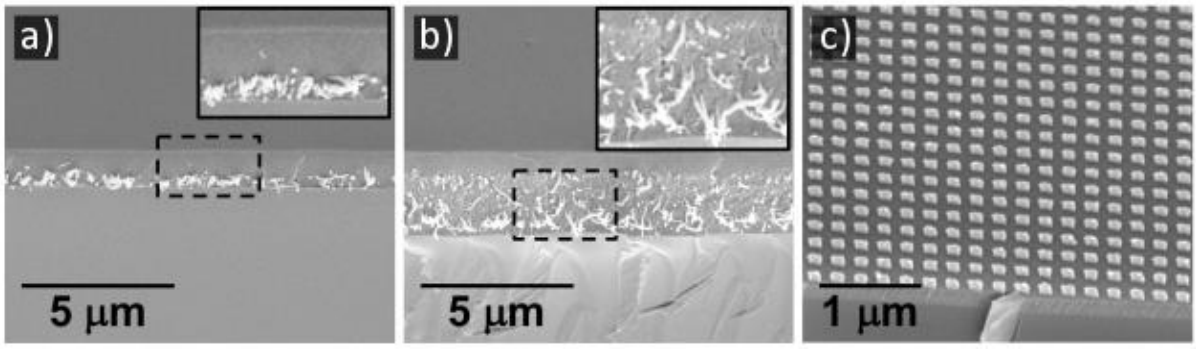

Figure 4. SEM images of MWCNT films prepared using chemical vapour deposition (CVD) with a PDMS over-coat using the following CVD growth times: (a) 1 minute growth time, (b) 3 minute growth time. (c) SEM image of an AuNP array prior to PDMS coating. Adapted with permission[37]. Copyright 2010, AIP Publishing LLC.

Bottom-up fabrication methods can be used to create PDMS composites using exotic nanomaterials such as MWCNTs. Unlike all-in-one fabrication methods, these expensive nanomaterials are not directly incorporated into quick cure polymers, thereby minimising wastage. Here, MWCNTs can be coated onto surfaces using techniques such as CVD or dip-coating methods, with PDMS applied as an over-coat by spin-coating or dip-coating. Using a bottom-up-fabrication method, Baac *et al*. coated glass substrates such as planar fused silica[37] and concave lens[15] surfaces with MWCNTs by CVD. MWCNT coating thicknesses on the fused silica surfaces were optimised for ultrasound generation and high frequency performance at 2.6 µm (*ca.* 80% optical absorption)[37]. PDMS was applied using spin-coating and was found to increase the damage threshold of the ultrasound transmitters[16]. The performance of the MWCNT-PDMS composite (Figure 4 (a), (b)) was compared with an AuNP-PDMS composite that was fabricated using a metal transfer method (Figure 4 (c))[52] and it was found the former outperformed the AuNP composite in both ultrasound generation efficiency and bandwidth[37].

A focused ultrasound source was fabricated by creating MWCNT-PDMS composite coatings on a concave lens surface using CVD methods for MWCNT deposition and spin-coating for PDMS. The MWCNTs demonstrated an optical absorption between 60 – 70% and this was increased to greater

than 85% by over-coating with a thin gold layer[15]. The coated lenses had low *f*-numbers (0.92, 0.96) and focal gains of 54 and 100 at an ultrasound frequency of 15 MHz. At the focal point, these coated lenses generated a maximum measured negative ultrasound pressures of *ca.* 13.3 MPa[15]. High negative pressures are crucial for achieving cavitation and in this study, the negative pressures achieved were sufficient to cause microfragmentation by cavitation[15]. More recently, the same group used a lower f-number MWCNT-PDMS coated lens (0.61) to achieve a higher focal gain of 220 at an ultrasound frequency of 15 MHz[40]. This device had a tight focus (90 µm x 200 µm at 9.2 mm) which enabled the first demonstration of free field cavitation. Using this lens as a sonic scalpel, Lee *et al*. achieved a negative pressure greater than 30 MPa. This was sufficient to demonstrated cavitation cutting of tissue-mimicking phantoms and a swine eyeball[53] with a resolution of 50 µm. These types of devices enable therapeutic applications such as tissue ablations (tumours) or breaking up small blood clots through ultrasonic thrombolysis.

With bottom-up methods it can be important to integrate the polymer and the absorbing layer. Baac *et al.* investigated the integration of PDMS into an underlying MWCNT layer[16]. It was found that dense MWCNT networks resulted in poor PDMS infiltration through the MWCNT layer. This was thought to reduce the composite's adhesion to the substrate, as well as the thermal transmission from the MWCNTs to the PDMS host[16]. With lower density MWCNT films, better infiltration of PDMS through the MWCNTs enabled greater contact between the PDMS and the substrate, which increased the laser damage threshold and thus the maximum attainable ultrasound pressures[16].

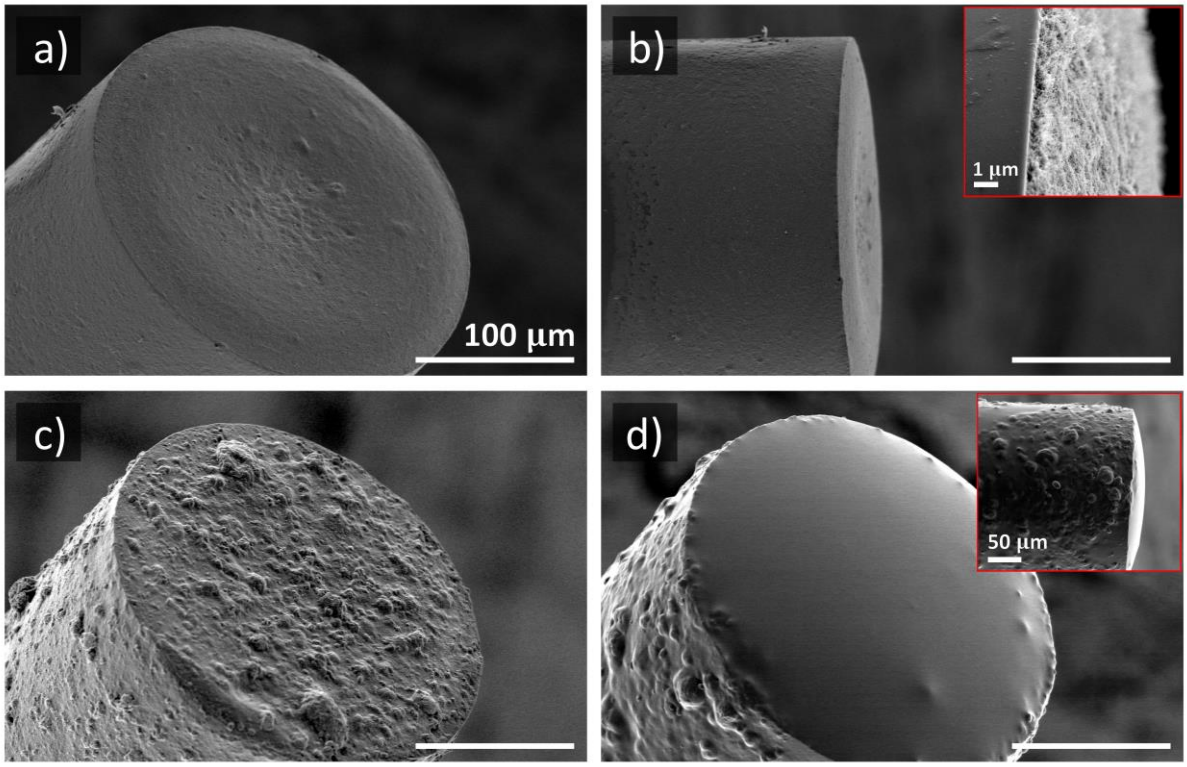

Figure 5. SEM images of MWCNT and MWCNT-PDMS coated optical fibres prepared using a bottom-up fabrication method (scale bar: 100 µm). (a) and (b) Fibres coated using a MWCNT-xylene solution that have a coffee-ring coating morphology (inset scale bar: 1 µm). (c) Fibre coated with a MWCNT-gel. (d) Fibre coated with MWCNT-gel-PDMS composite (inset scale bar: 50 µm). Adapted under the terms of the CC-BY-4 license.[20] Copyright 2016, Noimark *et al.*

To create fibre-optic ultrasound transmitters for miniature imaging probes, methods for efficiently coating small, temperature-sensitive surfaces with MWCNT films have been developed. Although CVD is an efficient method to coat large planar surfaces with MWCNT films, it requires high temperatures unsuited to optical fibres which typically comprise temperature-sensitive polymer coatings. Noimark *et al*. developed a solution-based bottom-up fabrication method to coat optical fibres using three types of MWCNT-PDMS coatings[20]. MWCNTs were functionalised using an oleylamine-functionalised pyrene ligand, and this xylene-based MWCNT formulation was used to prepare a MWCNT gel formulation[20]. These formulations can be deposited onto a range of substrates by dip-coating or spin-coating to form optically absorbing coatings with small thicknesses. Using these two MWCNT formulations, dip-coating methods were used to deposit the MWCNT

coatings onto optical fibres, after which they were dip-coated with PDMS to form two distinct MWCNT-PDMS composite coatings (Figure 5)[20]. Notably, the coating created with the xylene-based MWCNT formulation showed a coffee-ring drying effect with a maximum coating thickness of less than 1 µm, whereas the use of the MWCNT gel resulted in more uniform coatings across the fibre tip. The MWCNT-PDMS coated optical fibres formed highly miniaturised ultrasound transmitters and generated pressures of up to 4.5 MPa at a distance of 3 mm from the coating, with corresponding bandwidths of around 30 MHz[20]. Using the MWCNT gel-PDMS composite, an all-optical ultrasound imaging probe was fabricated to image swine tissue[20]. The probe comprised the composite coated fibre for ultrasound transmission and a Fabry-Pérot fibre-optic sensor for ultrasound reception[54]. Fabry-Pérot sensors are widely used for all-optical ultrasound imaging due to their high sensitivity (noise equivalent pressure < 200 Pa) and diminutive acoustic element size (tens of microns)[46,51,55–57]. The probe was mounted on a motorised two-axis translation stage to scan three spatially distinct lines to construct cross-sectional images through a swine aorta. Imaging depths exceeded the tissue thickness; the broad bandwidths resulted in high-resolution images that showed clinically relevant detail such as a side branch and distinct tissue layers[20].

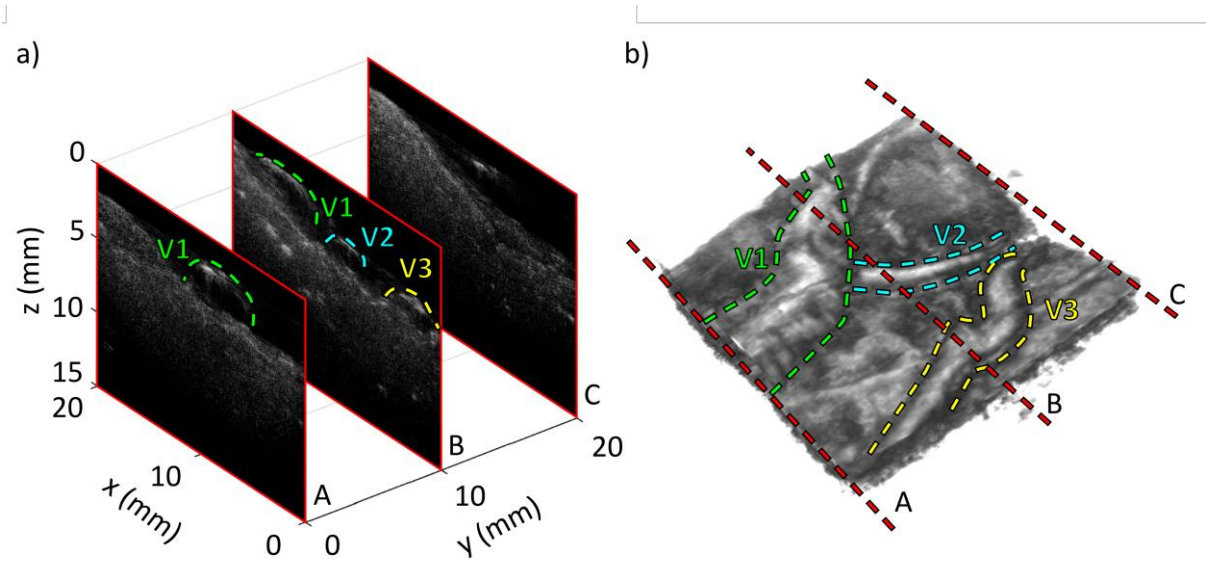

Figure 6: 3D all-optical ultrasound image of a section of normal term human placenta *ex vivo.* Ultrasound transmission was performed with a MWCNT-gel/PDMS coating; reception, with a Fabry-Pérot fibre-optic

sensor. (a) Cross-sections through human placenta (*x, y*: lateral distance; *z*: depth). (b) 3D rendering of the reconstructed all-optical ultrasound. Surface blood vessels are outlined with dashed lines and labelled V1, V2, and V3.

Three-dimensional ultrasound imaging can be performed by scanning an imaging probe across a two-dimensional grid. Here, for the first time, an *ex vivo* normal term human placenta tissue was imaged in 3D using all-optical ultrasound (experimental details are in Section 3, Supporting Information). In the imaging probe, a MWCNT gel-PDMS coating on an optical fibre served as the ultrasound transmitter. Mechanical raster scanning of the imaging probe was time consuming (> 4 hours). Human placental tissue was chosen as an imaging target due to its feature-rich vascular surface and potential applications in fetal surgery. The resulting reconstructed 3D image showed surface and subsurface vasculature (Figure 6), which are tissue structures of interest in photocoagulation for treatment of twin-to-twin-transfusion syndrome. Whilst these high acquisition times are incompatible with surgical imaging, there is strong potential to achieve a real-time imaging device, for instance by applying coatings to optical fibre bundles for ultrasound sources that can be rapidly translated without the need for mechanical motion[56].

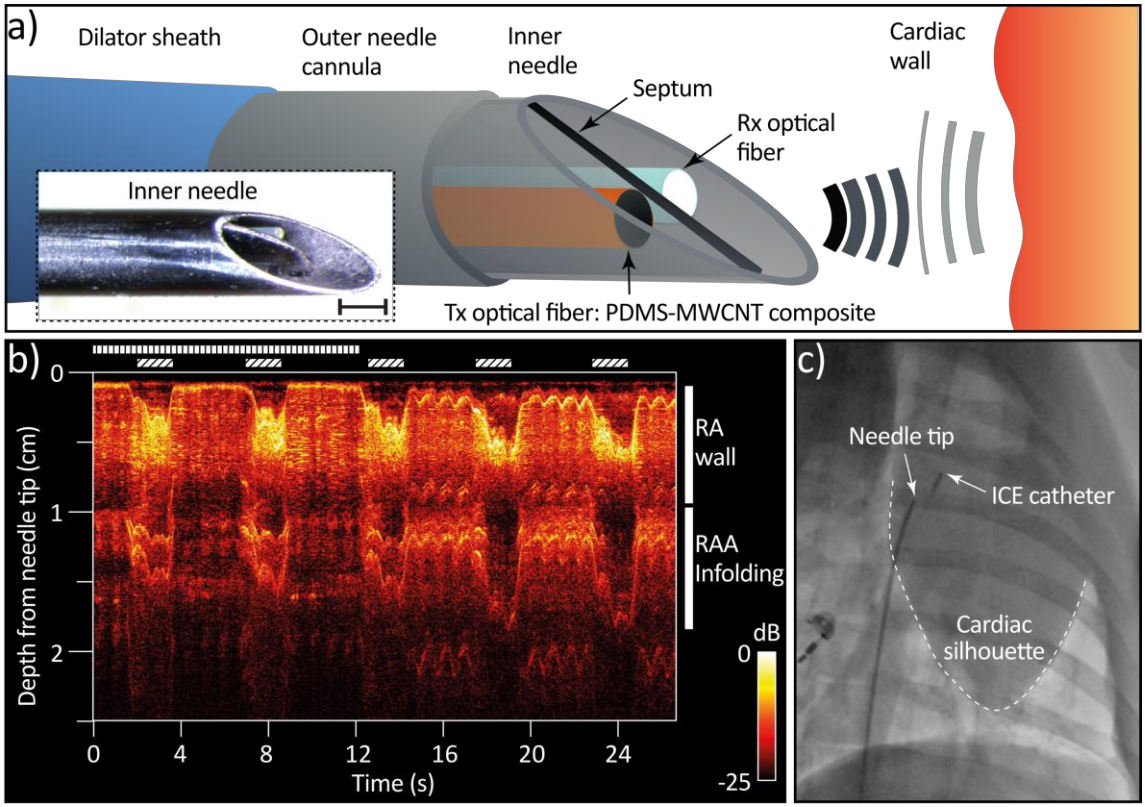

Figure 7. (a) Schematic of a needle with integrated optical ultrasound transmitter (Tx optical fiber) and optical ultrasound receiver (Rx optical fiber) used for real-time imaging *in vivo.* Scale bar: 500 µm. (b) Real-time M-mode all-optical ultrasound image acquired in the right atrium (RA) of a swine with needle pointed anteriorly. The needle was initially held against the RA wall (vertical bars). Diagonal bars indicate movement caused by mechanical ventilation. Right atrial appendage (RAA) infolding and motion was visible beyond the RA wall. (c) Medical X-ray fluoroscopy imaging showing needle location whilst imaging was performed. Adapted under the terms of the CC-BY-4 license.[23] Copyright 2017, Finlay *et al*.

Recently, all-optical ultrasound imaging has been used for real-time image guidance of a minimally invasive surgical procedure *in vivo*. In particular, a sensing device was fabricated for use in transseptal puncture, a commonly performed medical procedure to gain access to the left side of the heart[23]. The ultrasound probe comprised a MWCNT gel-PDMS coated transmitter and a Fabry-Pérot fibre-optic receiver that was built into a section of metal tubing to fit inside a commercial transseptal puncture needle (Figure 7 (a)). Real-time high-resolution M-mode ultrasound images of the heart anatomy, including atrial walls, aortic valves and septum, were acquired (Figure 7 (b), (c)).

Imaging at depths of up to 2.5 cm was achieved. This imaging paradigm shows promise for guiding intra-cardiac procedures. This demonstration of all-optical ultrasound in a challenging *in vivo* environment demonstrates the ability of the modality for use as a crucial guidance modality in minimally invasive interventions.

Using bottom-up fabrication, a broad range of surfaces have been coated for optical ultrasound generation including concave lenses[15], planar glass surfaces[37,39,42,44], and optical fibres[17,19,20]. Precise, micron-level control over the thickness of the optical absorbing layer can be achieved, leading to enhancements in the generated ultrasound bandwidth and corresponding spatial resolution. However, limitations of some bottom-up fabrication approaches include the scalability of some of the absorber deposition methods for high-throughput manufacturing, as well as the range of substrates that can be coated. For example, CVD is an efficient method for coating planar surfaces but lacks versatility for coating temperature sensitive miniature targets such as optical fibres. MWCNT-PDMS composites created using bottom-up fabrication highlight potential for use in biomedical ultrasound imaging; pre-clinical *ex vivo* and *in vivo* studies demonstrate that such all-optical imaging systems can achieve high-resolution imaging showing clinical relevant features.

2.3 Top-down Fabrication

Here we present novel top-down fabrication methods in which optical absorbers are incorporated into *pre-deposited* PDMS films on optical fibres. Incorporation of the optical absorbers can be achieved by several techniques including the diffusion of nanomaterials from solution into the pre-deposited PDMS coating[58,59] or by ion implantation[60]. The use of top-down methods allows for optimisation of the PDMS coating prior to inclusion of the absorber and recycling of absorber solutions which minimises wastage of expensive nanomaterials. Two PDMS composite optical ultrasound generators were fabricated: an AuNP-PDMS composite, and a crystal-violet (CV)-PDMS composite. These absorbers were chosen since they selectively absorb within a specific wavelength

region and allow for the transmission of light at other wavelengths. Notably, wavelength-selective coatings can also be fabricated using all-in-one and bottom-up methods. These wavelength-selective coatings will enable multi-modality devices for image guided therapies and interventions (Figure 8). Here, we use the term "multi-modality" in a broad sense to encompass multiple complementary functionalities, for example two imaging modalities that provide co-registered information about tissue, or concurrent imaging and energy delivery for therapy.

The top-down fabrication methods presented here were motivated by clinical interest in the development of miniature photoacoustic probes to guide minimally invasive procedures[61–65]. Photoacoustics provides information that is distinct from pulse-echo ultrasound imaging. With the latter, ultrasound is directly delivered to the tissue, resulting in contrast derived from spatial variations of acoustic impedance[66]. In photoacoustic imaging, it is excitation light that is delivered to the tissue, where it generates ultrasound. Therefore contrast is provided by the spatial variation in optical absorption and thus gives information on chromophore concentrations[24]. A key chromophore target for photoacoustic imaging is lipid, which has an optical absorption peak at 1210 nm. Lipid identification has important clinical implications as it can potentially be used to diagnose cardiovascular disease, which is typically caused by the build-up of fatty deposits in arteries. It is noteworthy that several studies have highlighted the value of pulse-echo ultrasound for the interpretation of photoacoustic signals. The former imaging modality can provide complementary microstructural information with which to interpret molecular information from the latter. Interventional imaging probes that combine these two modalities have been realised with electronic ultrasound transducers[67–73], however this approach can be challenging as it involves adding an optical pathway to existing piezoelectric probes, and the resulting devices can be bulky. An elegant solution is the integration of this technology into an all-optical ultrasound system, since the light delivery system for the photoacoustic imaging is already in place. Moreover, by engineering coatings

for optical ultrasound generation that allow for the transmission of a secondary wavelength, this technology can be extended to multi-modality imaging, sensing and therapy applications (Figure 8).

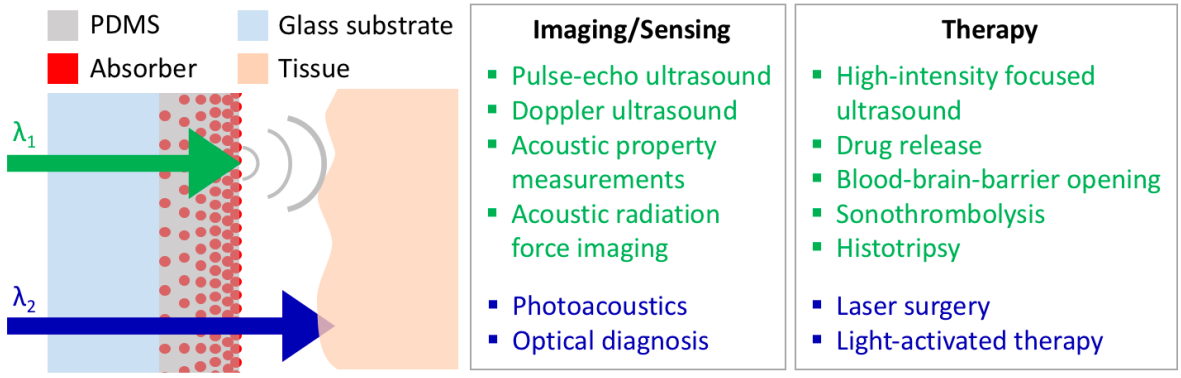

Figure 8: A schematic of a top-down PDMS composite coating for combined optical ultrasound generation and multi-modality devices, as well as examples of clinical applications. The wavelength-selective optical absorption of the composite allows for the functionality to vary with the light wavelength. At one wavelength (λ_1), light is substantially absorbed, which results in ultrasound transmission into tissue. At a second wavelength (λ_2), light is substantially transmitted into tissue. The broad classifications for the clinical use of transmitted light (λ_2) were obtained from Yun *et al.*[74]. Photoacoustics was listed separately for "optical diagnosis" due to its prominent role in this article.

Organic photosensitiser dyes are potentially well-suited to the development of coatings for multi-modality imaging due to their characteristic selective optical absorption. They are typically inexpensive and commercially available, and have been used for diverse applications including laser gain media[75,76], photodynamic therapy[77,78], and sensing[79]. For example, dye-PDMS composites have been fabricated by directly incorporating Sudan II or Nile Red into silicone rubber by mechanical mixing methods to fabricate waveguides for fluorescence detection and chemical sensing[79]. More recently, phenothiazine and triarylmethane photosensitiser dye-silicone composites have been created for the development of light-activated antimicrobial materials[58,80,81] and these composites are attractive candidates for optical ultrasound transmitters due to their high optical absorption within a narrow wavelength range. PDMS-dye incorporation methods include a "swell-encapsulation-shrink" strategy which results in the uniform encapsulation of dye molecules

within medical grade materials including silicone rubber and polyurethane[77,82,83], and a simple dipping method[58,78,80]. The latter is of particular interest as it achieves highly localised surface concentrations of the dye CV, with limited dye diffusion through the polymer bulk.

Gold nanoparticles (AuNPs) are also of significant interest for the development of coatings for combined ultrasound and photoacoustic imaging, as they exhibit wavelength dependent optical absorption. The distinct optical absorption bands exhibited arise from localised surface plasmon resonance[84] and the spectral location of these bands is dependent on the nanoparticle size and morphology[84–86]. AuNPs have been used as photoacoustic imaging contrast agents[87–89] and have existing applications in the development of coatings for optical ultrasound generation[17,41,51]; their wavelength-selective nature has been previously exploited to fabricate an integrated ultrasound transmitter-receiver[51]. Methods that have been used to develop AuNP-PDMS composites include direct mechanical mixing of PDMS with AuNPs (which were functionalised for improved dispersion)[90,91], and the *in situ* formation of AuNPs within PDMS by mixing the gold salt with the PDMS precursor[17,41] or submerging cured PDMS in a gold salt solution[59,92]. The *in situ* reduction method is a promising top-down approach for the development of PDMS composites for multi-modality imaging, as it enables high optical extinction between 530 and 550 nm[59,92]; the low optical absorption of these composites at near-infrared wavelengths enables the transmission of excitation light for photoacoustic imaging.

Using top-down fabrication methods, both CV-PDMS composite coatings and AuNP-PDMS composite coatings were formed on the distal ends of optical fibres (Section 1.1-1.2, Supporting Information). The CV-PDMS coatings were created by immersing a PDMS-coated optical fibre in a heated CV solution for extended periods of time, thereby allowing the dye to diffuse into the PDMS to achieve a large uptake of the dye. AuNP-PDMS composites were created on PDMS-coated optical fibres via *in situ* reduction of gold salt in a cured PDMS host[59,92,93]. Examination of the both the AuNP- and CV-

PDMS composite coatings using stereomicroscopy with through-fibre illumination (white light) showed the coatings had a purple colouration, which can be attributed to the wavelength specific absorption (Figure 9 (b), (d)). Analysis of the coatings using scanning electron microscopy (SEM) indicated that the AuNP-PDMS composites had smooth dome-like coatings covering the optical fibre end face, with a thickness up to 100 µm (Figure 9 (e), (f), (g), (h)). The SEM images of the CV-PDMS composites revealed much thinner coatings of 20 µm thickness, which can be attributed to the dilution of the PDMS dipping solution resulting in lower viscosity. The SEM also indicated the presence of debris on the CV-PDMS surface, which may have been caused by CV agglomeration on the PDMS.

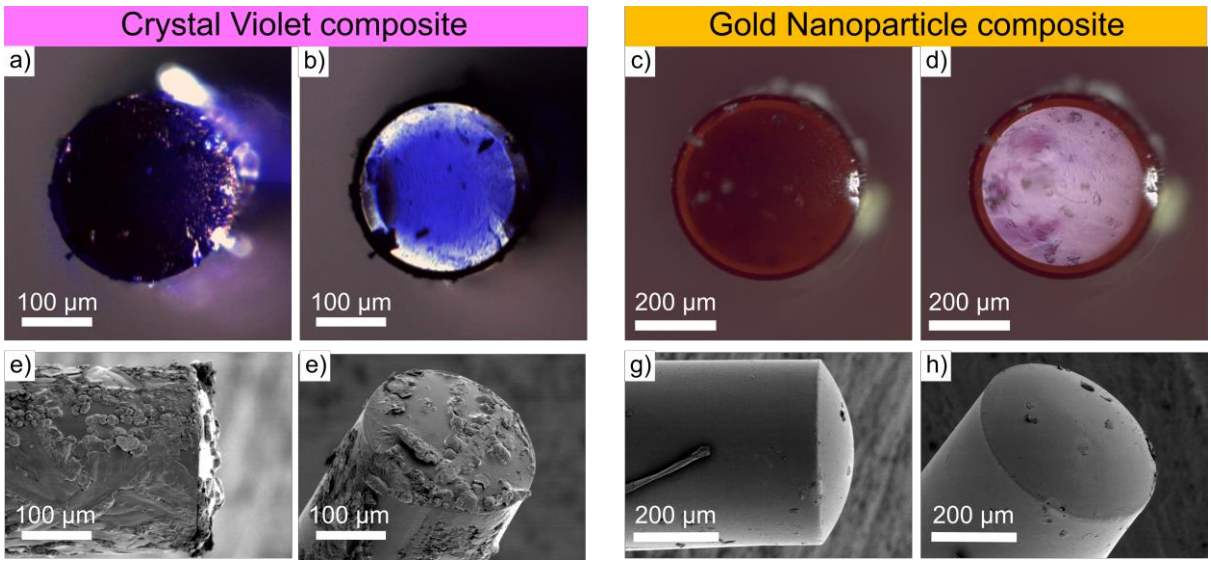

Figure 9: Stereomicroscope and SEM images of a CV-PDMS composite coating (left side) and a AuNP-PDMS composite (right side).

The optical properties of the AuNP-PDMS and the CV-PDMS composites were characterised to assess their suitability for multi-modality imaging. Their optical absorption spectra were measured using an integrating sphere (Section 2.1, Supporting Information). The CV-PDMS coating had high optical absorption within the region 500 – 620 nm, absorbing greater than 75% of the incident light (Figure 10 (a)), whereas the AuNP composites showed a narrower absorption range with absorption of 91%

of the incident light at 540 nm and 89% at 532 nm (Figure 10 (a)). For both composites, less than 10% of incident light was absorbed at longer wavelengths (> 850 nm). The small optical absorption peak at 1185 nm originates from the PDMS[26]. These spectral features highlight the potential of these composites for multi-modality imaging and therapeutic applications (Figure 8).

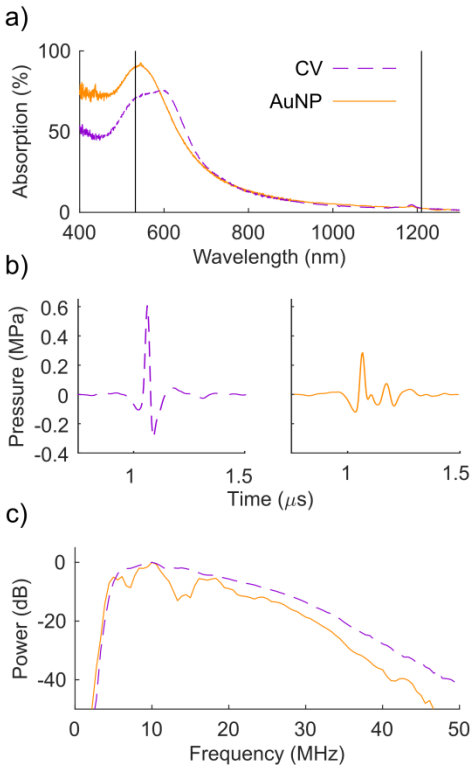

Figure 10: (a) Optical absorption spectrum of the crystal violet (dashed purple line) and AuNP (solid gold line) composite coatings. Black lines indicate laser excitation wavelengths for ultrasound (532 nm) and photoacoustic imaging (1210 nm). (b) Ultrasound time-series generated by crystal violet and AuNP composite coatings, measured at a distance of 1.5 mm from the coating. (c) Ultrasound power spectra generated by crystal violet and AuNP composite coatings.

For diagnostic ultrasound imaging, it is beneficial to have high ultrasound pressures and wide bandwidths for good tissue penetration and high-resolution imaging. The ultrasound generation of the two composites was characterised in terms of their peak-to-peak pressures, measured at a distance of 1.5 mm from the coating surface (Figure 10 (b) and Section 2.2, Supporting Information).

For an incident optical fluence of 86.3 mJ/cm^2, the CV-PDMS composites achieved peak-to-peak pressures up to 0.90 MPa. By comparison, the AuNP-PDMS composite was 29% less efficient (peak-to-peak pressure: 0.41 MPa; incident optical fluence of 55.3 mJ/cm^2). The AuNP-PDMS composites were found to be photo-stable (Section 2.3, Supporting Information). Conversely, the CV-PDMS composites displayed poor photo-stability which resulted in an 80% reduction in the generated ultrasound pressures within 15 minutes of constant exposure at 100 Hz. The photobleaching of the CV-PDMS coatings poses concerns over the viability of these composites for clinical ultrasound imaging, which may require up to several hours of device usage in complicated surgical procedures. Future research will include the creation of composites comprised of PDMS and absorbers such as quantum dots that are less prone to photobleaching than organic dyes[94].

The achievable resolution for imaging applications is related to the generated ultrasound frequency bandwidth; the wider the bandwidth the higher the image resolution. The -6 dB ultrasound bandwidths for the CV-PDMS and AuNP-PDMS composites were measured as 15.1 MHz and 4.5 MHz, respectively (Figure 10 (c)). These values are comparable to conventional ultrasound imaging systems, and to those of the MWCNT-PDMS coating prepared using an all-in-one method that was used for swine vascular tissue imaging[46]. The reduced bandwidth of the ultrasound generated by the AuNP-PDMS coating may be due to its greater coating thickness, or due to ultrasound reflections within the coating. The latter effect is a consequence of the top-down fabrication process and is caused by the confinement of the AuNPs within a thin region at the PDMS surface[92]. Here, the ultrasound waves generated within the optically absorbing region propagate both forwards (towards a target) and backwards (towards the glass optical fibre surface). The ultrasound waves propagating backwards through the composite are reflected at the optical fibre end face and interfere with the forward propagating waves, which contributes to non-uniformity of the frequency spectrum. Nevertheless, the overall shapes of the frequency spectra for the CV-PDMS and AuNP-PDMS composites are similar in form, and their -20 dB bandwidths are comparable (30.9 MHz and 27.4

MHz, respectively). These bandwidths can be increased further (for higher imaging resolution) by reducing the thickness of the optically absorbing composite region[27,28]. Strategies to achieve thinner coatings include the use of organic solvents such as toluene and xylene to reduce the PDMS thickness. For the AuNP-PDMS composite, this would be doubly advantageous since thinning the PDMS layer sufficiently would decrease the distance between the AuNP region and the underlying glass fibre, thereby pushing reflection interference features in the power spectrum to higher frequencies. However, it is noteworthy that the ultrasound pressures and bandwidths generated by these selectively absorbing coatings compare favourably to the literature (Table 2), including those fabricated by Colchester *et al*. that achieved pulse-echo images of *ex vivo* swine tissue with clinically relevant detail[46].

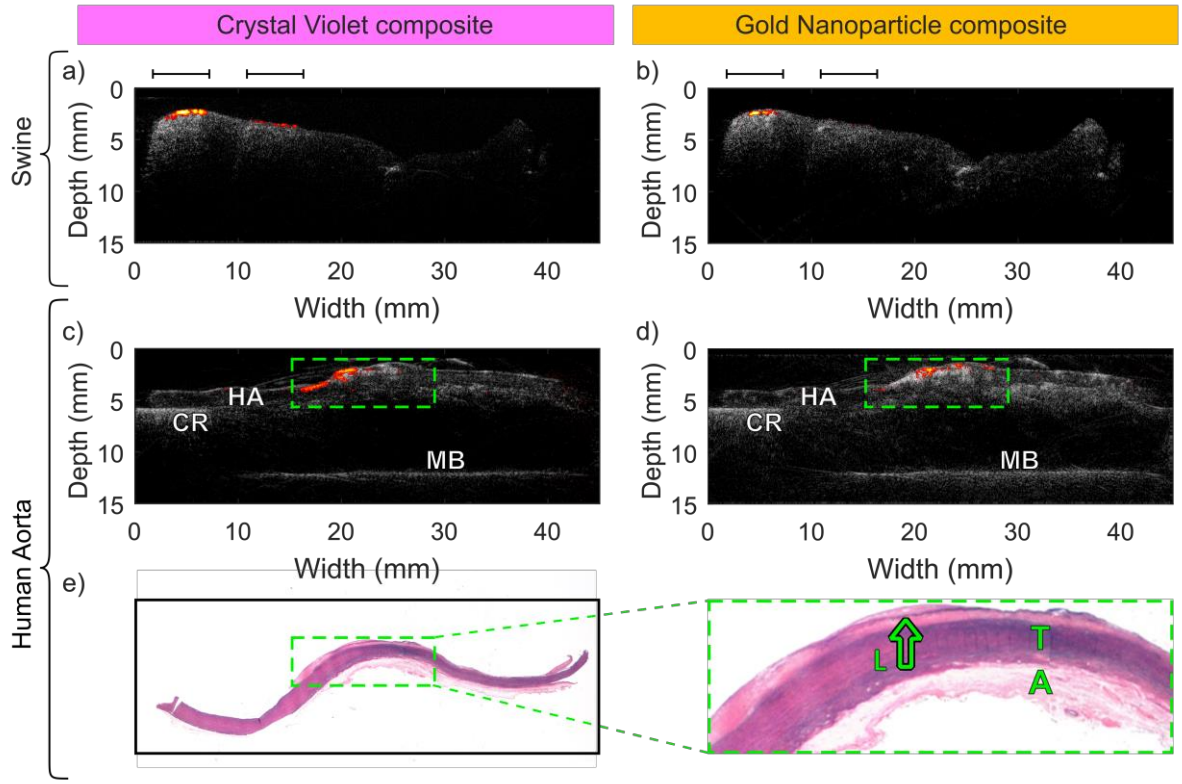

Figure 11: (a-d) All-optical ultrasound and photoacoustic images acquired using a CV-PDMS composite transmitter (left side) and an AuNP-PDMS composite transmitter (right side). Photoacoustic signals were overlaid in colour onto the grayscale ultrasound images. (a,b) *Ex vivo* swine abdominal tissue, in which fatty regions (black bars) were interspersed with muscle. (c,d) *Ex vivo* diseased human aorta tissue (HA), which was

positioned on a cork ring (CR) and a metal base (MB) during imaging. (e) Histological cross-section (haematoxylin and eosin stain) of the imaged human aorta tissue. In the magnified region (dashed green box), lipid pools (L; arrow) were apparent in the intima above the tunica media (T) and adventitia (A). The spatial locations of these lipid pools corresponded well to the locations of the photoacoustic signals (c,d; dashed green boxes).

The optical and ultrasound properties of both top-down fabricated composites are well-suited for combined all-optical ultrasound and photoacoustic imaging. These ultrasound transmitters were integrated into an ultrasound/photoacoustic imaging probe in apposition with a Fabry-Pérot fibre-based ultrasound receiver[95], similar to that previously described for all-optical ultrasound imaging[46] (Section 3, Supporting Information). Ultrasound generation was achieved using a 532 nm excitation source, and a 1210 nm laser was used for photoacoustic imaging. This wavelength was chosen as it coincides with a peak in the lipid absorption spectrum[24]. To validate this technology for applications in combined ultrasound and photoacoustic imaging, two samples were imaged; (i) a slice of *ex vivo* swine abdominal tissue and (ii) a section of *ex vivo* diseased human aorta, with ultrasound and photoacoustic images acquired along the same plane (Figure 11 (a), (b)). The swine abdominal tissue was selected as it has large fatty regions, which are useful targets to determine the efficacy of the probes for photoacoustic imaging of lipid (Supporting information Figure 4 (g)). Both probes achieved high-resolution ultrasound imaging and revealed clinically relevant information. Interestingly, the ultrasound signal from the fatty regions showed up as brighter than the surrounding tissue. The ultrasound image of the *ex vivo* swine abdominal tissue that was acquired using the CV-PDMS transmitter showed a reduction in SNR across the image width that was consistent with the observation that the composite had poor photo-stability (Supporting information, Figure 1): reduced ultrasound pressures with irradiation time were apparent. However, for the *ex vivo* diseased human aorta sample imaged using the CV-PDMS transmitter, the signal was sufficient for imaging the entire section, despite a reduction in SNR across the image width.

Conversely, the probe comprised of an AuNP-PDMS composite transmitter showed consistent signal strength across both images (Figure 11 (b)), which derived from the photo-stability of this coating and underlined its suitability for ultrasound imaging applications in minimally-invasive procedures.

Photoacoustic imaging demonstrated the efficacy of the AuNP-PDMS and the CV-PDMS composites for achieving clinically relevant molecular information. Imaging of the swine abdominal tissue showed the first two fatty regions, with good registration between the fatty regions observed in the photoacoustic signals and the photograph of the tissue (Supporting Information Figure 4). However, the performance of the two probes differed. Whilst photoacoustic imaging using the CV-PDMS integrated probe clearly showed both fatty regions, the photoacoustic image of the second fatty region was barely visible in the case of the AuNP-PDMS integrated probe. This may have been due to the larger fibre core diameter of the AuNP-PDMS transmitter, which resulted in a reduced optical fluence for generating the photoacoustic signal, and thus a decrease in signal intensity. The reduced fluence is not a limitation of the AuNP-PDMS composite, but rather, the fibre core diameter chosen for the probe. The third lipid-rich region was not visible in the photoacoustic image obtained using either probe; the weaker signal was likely a consequence of the increased distance between the sample and the probe.

The two combined ultrasound/photoacoustic imaging probes were subsequently used to image an excised vessel section of diseased human aorta, harvested from a patient with cardiovascular disease. Both ultrasound and photoacoustic images were acquired along the same plane and the resulting images from both probes showed clinically relevant ultrasound and photoacoustic detail. Despite the differences in the ultrasound properties (pressure and bandwidth) of the two coatings, the acquired ultrasound images were comparable. For both composites, the full thickness of the aorta sample was resolved with ultrasound imaging, as was the cork ring the vessel was mounted on (leftmost side of ultrasound images). In addition, the metal base plate was visualised at a total

imaging depth of at least 15 mm. As seen in the images acquired of the abdominal swine tissue, a bright region in the US image was observed and identified as plaque using photographs (Supporting Information Figure 5 (g)) and histology (Figure 11 (e)). Moreover, the photoacoustic signal generated originated from a lipid-rich region in the plaque, which corresponded to an area of brightness in the ultrasound image and the presence of fat at this location was confirmed with photographs (Supporting information Figure 5 (g)) and histology (Figure 11 (e)). To the authors' knowledge, these are the first all-optical pulse-echo ultrasound and photoacoustic images of a human vessel, and they highlight the potential of this multi-modality imaging platform for diagnostic clinical applications.

Top-down fabrication is well-suited to the development of novel materials for optical ultrasound generation. In this work, top-down fabrication of wavelength-selective materials for multi-modality ultrasound and photoacoustic imaging was demonstrated. The fabricated composites were utilised for the first demonstration of all-optical ultrasound and photoacoustic imaging of human tissue using a multi-modality fibre-optic probe. This technology also sets the stage for combined diagnostic and therapeutic applications (Figure 8); laser light transmitted through the coating and delivered to the tissue could be used for ultrasound-guided ablation. Alternatively, using multiple transmitted wavelengths, spectroscopy can be done to identify tissue types and return functional information such as tissue oxygenation[24].

3 Future Directions

This article discusses three distinct fabrication methods for the development of highly optically absorbing PDMS composites and their applications in optical ultrasound generation. This field has benefitted greatly from the wealth of research undertaken on the development of PDMS composites in other fields. For instance, plasma bonding techniques used in microfluidics[96] may be useful to improve adhesion between glass substrates and PDMS composites used in optical ultrasound

generation. A more comprehensive understanding of the thermal-coupling between the absorbers and the PDMS hosts, and its effect on the generated ultrasound, may lead to coatings with increased ultrasound efficiencies and wider bandwidths. Other coating properties such the specific heat capacity and the speed of sound could also be optimised for optical ultrasound generation.

PDMS can be manipulated to form micron or sub-micron scale features with techniques such as laser direct writing[97] and UV lithography[98], or with spin coating over templates[99,100]. Micro-structured PDMS composites can also be prepared by nanoskiving[101,102]. The resulting two and three dimensional structured PDMS coatings have a wide range of potential applications in optical ultrasound generation; sub-micron structuring may enable accurate shaping of the acoustic field, and sub-wavelength feature sizes may help achieve the fabrication of acoustic metasurfaces[103], paving the way to a broad range of new optical ultrasound devices. On a larger scale, PDMS can be 3D printed to form a range of structures[104], and to generate custom sound fields similar to those demonstrated by Brown *et al*., where a structured surface was used to shape the transmitted ultrasound field[105]. These fabrication techniques can also be used to create ultrasound generating lenses, similar to those designed by Baac *et al*.[15] and Alles *et al*.[106]. Using sub-micron fabrication techniques, these simple curved lens structures can be extended to Fresnel lenses[107], allowing for the development of micron-thick devices. The resulting focused optical ultrasound generators have potential applications in diverse clinical specialities such as liver, prostate, and bladder surgery, neurosurgery, and obstetrics and gynaecology[108], as well as in targeted drug delivery. Alternatively, PDMS can be manipulated to form deformable lenses[109,110], allowing for the creation of optical ultrasound transmitters with a tuneable focus, that can be reconfigured for imaging and high intensity focused ultrasound applications.

Controlled patterning of an absorbing composite can also be used to fabricate holographic ultrasound generating devices[111,112]. Here, patterned optical absorption profiles are used to

generate custom wave fields and foci. A single holographic generation field is used to produce a single ultrasound field profile. This could be extended by using wavelength specific absorbers, allowing several field profiles to be encoded in a single thin membrane and excited using different optical wavelengths. Holographic ultrasound generation may open avenues into non-destructive testing, diagnostics and object manipulation[113].

4. Conclusion

PDMS is a material that is well suited to optical ultrasound generation but there remain many directions along which it can be optimised. Current fabrication methods, which we classified into "all-in-one", "bottom-up" and "top-down" methods, have led to ultrasound generation surfaces that yield pressures and bandwidths equal or superior to conventional ultrasonic transducers. These methods have different types of advantages; for instance, all-in-one coatings can be advantageous in terms of simplicity. Bottom-up methods can be used to minimise wastage of nanomaterials and coating thicknesses. Here, we used a bottom-up MWCNT-PDMS composite to acquire of the first 3D all-optical ultrasound image of *ex vivo* human tissue. We also presented two novel top-down methods using both organic and inorganic optical absorbers. These composites were used for multi-modality imaging of diseased human tissue. Their wavelength-selective absorption allowed for ultrasound and photoacoustic imaging to be performed, to obtain both structural and molecular contrast. In the future, PDMS composites could provide a broad range of sensing and therapeutic functionalities. With widespread interest in PDMS composites in biomedicine, recent advances could be readily translated for the development of new generations of optical ultrasound generators.

Acknowledgements

A placenta was collected with written informed consent after a caesarean section delivery at University College Hospital (UCH). The Joint UCL/UCLH Committees on the Ethics of Human Research

approved the study (14/LO/0863). The aortic valves implants were provided by Oxford Heart Valve Bank at John Radcliffe Hospital Oxford. Samples were obtained when AV implants had been rejected for use as homograft implants. All samples were collected under approved ethical guide lines with informed consent that allowed us to anonymously analyse the tissues. Ethical approval has been obtained from the Health Research Authority - NRES Committee London (10/H0724/18) to research tissue from organ donors.

This work was supported by Innovative Engineering for Health award by the Wellcome Trust (No. WT101957) and the Engineering and Physical Sciences Research Council (EPSRC) (No. NS/A000027/1, No. EP/N509577/1, No. EP/N021177/1), by Starting Grants from the European Research Council (ERC-2012-StG, Proposal No. 310970 MOPHIM; and ERC-2015-StG, Proposal No. 679891, InteGlazing), National Institute for Health Research UCL Biomedical Research Centre, Ramsay Memorial Trust (award of a fellowship), and by University College London through the Overseas Research Scholarship and Faculty of Engineering Dean's Prize and by the UCL EPSRC Centre for Doctoral Training in Medical Imaging (EP/L016478/1).

We gratefully acknowledge technical support from Olumide Ogunlade, Robert Ellwood, and Bradley Treeby from the Department of Medical Physics and Biomedical Engineering at UCL.

Bibliography

[1] Y. R. Jeong, H. Park, S. W. Jin, S. Y. Hong, S.-S. Lee, J. S. Ha, *Adv. Funct. Mater.* **2015**, *25*, 4228.
[2] N. Lu, C. Lu, S. Yang, J. Rogers, *Adv. Funct. Mater.* **2012**, *22*, 4044.
[3] T. Yamada, Y. Hayamizu, Y. Yamamoto, Y. Yomogida, A. Izadi-Najafabadi, D. N. Futaba, K. Hata, *Nat. Nanotechnol.* **2011**, *6*, 296.
[4] C. Fang, L. Shao, Y. Zhao, J. Wang, H. Wu, *Adv. Mater.* **2012**, *24*, 94.
[5] L. Liu, S. Peng, W. Wen, P. Sheng, *Appl. Phys. Lett.* **2007**, *91*.
[6] R. Ding, H. Liu, X. Zhang, J. Xiao, R. Kishor, H. Sun, B. Zhu, G. Chen, F. Gao, X. Feng, J. Chen, X. Chen, X. Sun, Y. Zheng, *Adv. Funct. Mater.* **2016**, *26*, 7708.
[7] C. K. Jeong, K. Il Park, J. Ryu, G. T. Hwang, K. J. Lee, *Adv. Funct. Mater.* **2014**, *24*, 2620.
[8] J. Loomis, B. King, T. Burkhead, P. Xu, N. Bessler, E. Terentjev, B. Panchapakesan, *Nanotechnology* **2012**, *23*, 45501.
[9] D. Qin, Y. Xia, G. M. Whitesides, *Nat. Protoc.* **2010**, *5*, 491.
[10] J. Hong, J. Lee, C. K. Hong, S. E. Shim, *Curr. Appl. Phys.* **2010**, *10*, 359.
[11] X. Niu, S. Peng, L. Liu, W. Wen, P. Sheng, *Adv. Mater.* **2007**, *19*, 2682.

[12] J. Zhou, H. Yan, Y. Zheng, H. Wu, *Adv. Funct. Mater.* **2009**, *19*, 324.
[13] H. Cong, T. Pan, *Adv. Funct. Mater.* **2008**, *18*, 1912.
[14] X. Li, W. Wu, Y. Chung, W. Y. Shih, W.-H. Shih, Q. Zhou, K. K. Shung, *IEEE Trans. Ultrason. Ferroelectr. Freq. Control* **2011**, *58*, 2281.
[15] H. W. Baac, J. G. Ok, A. Maxwell, K.-T. Lee, Y.-C. Chen, A. J. Hart, Z. Xu, E. Yoon, L. J. Guo, *Sci. Rep.* **2012**, *2*, 989.
[16] H. W. Baac, J. G. Ok, T. Lee, L. Jay Guo, *Nanoscale* **2015**, *7*, 14460.
[17] X. Zou, N. Wu, Y. Tian, X. Wang, *Opt. Express* **2014**, *22*, 18119.
[18] R. J. Colchester, C. a. Mosse, D. I. Nikitichev, E. Z. Zhang, S. West, P. C. Beard, I. Papakonstantinou, A. E. Desjardins, In *Proc. of SPIE, Photons Plus Ultrasound: Imaging and Sensing*; Oraevsky, A. A.; Wang, L. V., Eds.; 2015; Vol. 9323, p. 932321.
[19] R. J. Colchester, C. A. Mosse, D. S. Bhachu, J. C. Bear, C. J. Carmalt, I. P. Parkin, B. E. Treeby, I. Papakonstantinou, A. E. Desjardins, *Appl. Phys. Lett.* **2014**, *104*, 173502.
[20] S. Noimark, R. J. Colchester, B. J. Blackburn, E. Z. Zhang, E. J. Alles, S. Ourselin, P. C. Beard, I. Papakonstantinou, I. P. Parkin, A. E. Desjardins, **2016**, 1.
[21] S.-L. Chen, *Appl. Sci.* **2016**, *7*, 25.
[22] B. T. Cox, P. C. Beard, *J. Acoust. Soc. Am.* **2005**, *117*, 3616.
[23] M. C. Finlay, C. A. Mosse, R. J. Colchester, S. Noimark, E. Z. Zhang, S. Ourselin, P. C. Beard, R. J. Schilling, I. P. Parkin, I. Papakonstantinou, A. E. Desjardins, *Light Sci. Appl.* **2017**, *In Press*.
[24] P. Beard, *Interface Focus* **2011**, *1*, 602.
[25] N. Bowden, W. T. S. Huck, K. E. Paul, G. M. Whitesides, *Appl. Phys. Lett.* **1999**, *75*, 2557.
[26] D. K. Cai, A. Neyer, R. Kuckuk, H. M. Heise, *Opt. Mater. (Amst).* **2008**, *30*, 1157.
[27] E. J. Alles, J. Heo, S. Noimark, R. J. Colchester, I. P. Parkin, H. Won Baac, A. E. Desjardins, In *Proceedings of IEEE Ultrasonics Symposium 2017 (in print)*; 2017.
[28] T. Buma, M. Spisar, M. O'Donnell, *IEEE Trans. Ultrason. Ferroelectr. Freq. Control* **2003**, *50*, 1161.
[29] M. Xu, L. V. Wang, *Rev. Sci. Instrum.* **2006**, *77*, 41101.
[30] A. L. McKenzie, *Phys. Med. Biol.* **1990**, *35*, 1175.
[31] J. E. Mark, *Polymer Data Handbook*; Oxford University Press, 2009.
[32] J. K. Tsou, J. Liu, A. I. Barakat, M. F. Insana, *Ultrasound Med. Biol.* **2008**, *34*, 963.
[33] D. Kacik, P. Tatar, I. Martincek, In *2014 ELEKTRO*; IEEE, 2014; pp. 662–665.
[34] Z. Cai, W. Qiu, G. Shao, W. Wang, *Sensors Actuators A Phys.* **2013**, *204*, 44.
[35] D. Carugo, J. Owen, C. Crake, J. Y. Lee, E. Stride, *Ultrasound Med. Biol.* **2015**, *41*, 1927.
[36] S. A. Goss, R. L. Johnston, F. Dunn, *J. Acoust. Soc. Am.* **1978**, *68*, 423.
[37] H. W. Baac, J. G. Ok, H. J. Park, T. Ling, S.-L. Chen, A. J. Hart, L. J. Guo, *Appl. Phys. Lett.* **2010**, *97*, 234104.
[38] T. Buma, M. Spisar, M. O'Donnell, In *IEEE transactions on ultrasonics, ferroelectrics, and frequency control*; 2003; Vol. 50, pp. 1065–1068.
[39] W.-Y. Chang, W. Huang, J. Kim, S. Li, X. Jiang, *Appl. Phys. Lett.* **2015**, *107*, 161903.
[40] T. Lee, J. G. Ok, L. J. Guo, H. W. Baac, *Appl. Phys. Lett.* **2016**, *108*, 104102.
[41] N. Wu, Y. Tian, X. Zou, V. Silva, A. Chery, X. Wang, *J. Opt. Soc. Am. B* **2012**, *29*, 2016.
[42] Y. Hou, J.-S. Kim, S. Ashkenazi, M. O'Donnell, L. J. Guo, *Appl. Phys. Lett.* **2006**, *89*, 93901.
[43] R. K. Poduval, S. Noimark, R. J. Colchester, T. J. Macdonald, I. P. Parkin, A. E. Desjardins, I. Papakonstantinou, *Appl. Phys. Lett.* **2017**, *110*, 223701.
[44] B.-Y. Hsieh, J. Kim, J. Zhu, S. Li, X. Zhang, X. Jiang, *Appl. Phys. Lett.* **2015**, *106*, 21902.
[45] T. Lee, L. J. Guo, *Adv. Opt. Mater.* **2017**, *5*, 1600421.
[46] R. J. Colchester, E. Z. Zhang, C. A. Mosse, P. C. Beard, I. Papakonstantinou, A. E. Desjardins, *Biomed. Opt. Express* **2015**, *6*, 1502.
[47] E. J. Alles, R. J. Colchester, A. E. Desjardins, *IEEE Trans. Ultrason. Ferroelectr. Freq. Control* **2016**, *63*, 83.
[48] T. Buma, M. Spisar, M. O'Donnell, *Appl. Phys. Lett.* **2001**, *79*, 548.
[49] Y. Hou, S. Ashkenazi, S.-W. Huang, M. O'Donnell, *IEEE Trans. Ultrason. Ferroelectr. Freq. Control* **2007**, *54*, 682.
[50] Y. Tian, N. Wu, X. Zou, H. Felemban, C. Cao, X. Wang, *Opt. Eng.* **2013**, *52*, 65005.
[51] Y. Hou, J.-S. J.-S. Kim, S. Ashkenazi, S.-W. S.-W. Huang, L. J. Guo, M. O'Donnell, M. O'Donnell, *Appl. Phys. Lett.* **2007**, *91*, 73507.
[52] M.-G. Kang, L. J. Guo, *J. Vac. Sci. Technol. B Microelectron. Nanom. Struct.* **2008**, *26*, 2421.
[53] T. Lee, W. Luo, Q. Li, H. Demirci, L. J. Guo, *Small* **2017**, 1701555.
[54] E. Z. Zhang, P. C. Beard, In *Proc. of SPIE, Photons Plus Ultrasound: Imaging and Sensing*; Oraevsky, A.

A.; Wang, L. V., Eds.; 2015; Vol. 9323, p. 932311.
[55] C. Sheaff, S. Ashkenazi, *IEEE Trans. Ultrason. Ferroelectr. Freq. Control* **2014**, *61*, 1223.
[56] E. J. Alles, N. Fook Sheung, S. Noimark, E. Z. Zhang, P. C. Beard, A. E. Desjardins, *Sci. Rep.* **2017**, *7*, 1208.
[57] E. Vannacci, L. Belsito, F. Mancarella, M. Ferri, G. P. Veronese, A. Roncaglia, E. Biagi, *Biomed. Microdevices* **2014**, *16*, 415.
[58] S. Noimark, J. Weiner, N. Noor, E. Allan, C. K. Williams, M. S. P. Shaffer, I. P. Parkin, *Adv. Funct. Mater.* **2015**, *25*, 1367.
[59] H. SadAbadi, S. Badilescu, M. Packirisamy, R. Wüthrich, *J. Biomed. Nanotechnol.* **2012**, *8*, 539.
[60] S. Rosset, M. Niklaus, P. Dubois, H. R. Shea, *Adv. Funct. Mater.* **2009**, *19*, 470.
[61] D. Piras, C. Grijsen, P. Schütte, W. Steenbergen, S. Manohar, *J. Biomed. Opt.* **2013**, *18*, 70502.
[62] J. M. Mari, W. Xia, S. J. West, A. E. Desjardins, *J. Biomed. Opt.* **2015**, *20*, 110503.
[63] A. Garcia-Uribe, T. N. Erpelding, A. Krumholz, H. Ke, K. Maslov, C. Appleton, J. A. Margenthaler, L. V Wang, *Sci. Rep.* **2015**, *5*, 15748.
[64] W. Xia, E. Maneas, D. I. Nikitichev, C. A. Mosse, G. Sato dos Santos, T. Vercauteren, A. L. David, J. Deprest, S. Ourselin, P. C. Beard, A. E. Desjardins, *Medical Image Computing and Computer-Assisted Intervention -- MICCAI 2015*; Navab, N.; Hornegger, J.; Wells, W. M.; Frangi, A. F., Eds.; Lecture Notes in Computer Science; Springer International Publishing: Cham, 2015; Vol. 9349.
[65] W. Xia, D. I. Nikitichev, J. M. Mari, S. J. West, R. Pratt, A. L. David, S. Ourselin, P. C. Beard, A. E. Desjardins, *J. Biomed. Opt.* **2015**, *20*, 86005.
[66] R. S. C. Cobbold, *Foundations of Biomedical Ultrasound*; Oxford University Press, 2006.
[67] K. Jansen, A. F. W. van der Steen, H. M. M. van Beusekom, J. W. Oosterhuis, G. van Soest, *Opt. Lett.* **2011**, *36*, 597.
[68] K. Jansen, G. van Soest, A. F. W. van der Steen, *Ultrasound Med. Biol.* **2014**, *40*, 1037.
[69] P. Wang, T. Ma, M. N. Slipchenko, S. Liang, J. Hui, K. K. Shung, S. Roy, M. Sturek, Q. Zhou, Z. Chen, J.-X. Cheng, *Sci. Rep.* **2014**, *4*, 6889.
[70] J. Hui, Q. Yu, T. Ma, P. Wang, Y. Cao, R. S. Bruning, Y. Qu, Z. Chen, Q. Zhou, M. Sturek, J.-X. Cheng, W. Chen, *Biomed. Opt. Express* **2015**, *6*, 4557.
[71] B. Wang, A. Karpiouk, D. Yeager, J. Amirian, S. Litovsky, R. Smalling, S. Emelianov, *Ultrasound Med. Biol.* **2012**, *38*, 2098.
[72] X. Ji, K. Xiong, S. Yang, D. Xing, *Opt. Express* **2015**, *23*, 9130.
[73] J. M. Yang, C. Favazza, J. Yao, R. Chen, Q. Zhou, K. K. Shung, L. V. Wang, *PLoS One* **2015**, *10*, e0120269.
[74] S. H. Yun, S. J. J. Kwok, *Nat. Biomed. Eng.* **2017**, *1*, 8.
[75] F. J. Duarte, R. O. James, *Opt. Lett.* **2003**, *28*, 2088.
[76] S. V. Frolov, Z. V. Vardeny, K. Yoshino, A. Zakhidov, R. H. Baughman, *Phys. Rev. B* **1999**, *59*, R5284.
[77] S. Noimark, M. Bovis, A. J. MacRobert, A. Correia, E. Allan, M. Wilson, I. P. Parkin, *RSC Adv.* **2013**, *3*, 18394.
[78] S. K. Sehmi, S. Noimark, J. C. Bear, W. J. Peveler, M. Bovis, E. Allan, A. J. MacRobert, I. P. Parkin, *J. Mater. B* **2015**, *3*, 6490.
[79] C. L. Bliss, J. N. McMullin, C. J. Backhouse, *Lab Chip* **2008**, *8*, 143.
[80] S. Noimark, E. Allan, I. P. Parkin, *Chem. Sci.* **2014**, *5*, 2216.
[81] S. Perni, C. Piccirillo, J. Pratten, P. Prokopovich, W. Chrzanowski, I. P. Parkin, M. Wilson, *Biomaterials* **2009**, *30*, 89.
[82] M. J. Bovis, S. Noimark, J. H. Woodhams, C. W. M. Kay, J. Weiner, W. J. Peveler, A. Correia, M. Wilson, E. Allan, I. P. Parkin, A. J. MacRobert, *RSC Adv.* **2015**, *5*, 54830.
[83] T. J. Macdonald, K. Wu, S. K. Sehmi, S. Noimark, W. J. Peveler, H. du Toit, N. H. Voelcker, E. Allan, A. J. MacRobert, A. Gavriilidis, I. P. Parkin, *Sci. Rep.* **2016**, *6*, 39272.
[84] S. Link, M. a. El-Sayed, *J. Phys. Chem. B* **1999**, *103*, 4212.
[85] C. J. Orendorff, T. K. Sau, C. J. Murphy, *Small* **2006**, *2*, 636.
[86] M. Hu, J. Chen, Z.-Y. Li, L. Au, G. V Hartland, X. Li, M. Marquez, Y. Xia, *Chem. Soc. Rev.* **2006**, *35*, 1084.
[87] Y.-S. Chen, W. Frey, S. Kim, K. Homan, P. Kruizinga, K. Sokolov, S. Emelianov, *Opt. Express* **2010**, *18*, 8867.
[88] D. Pan, B. Kim, L. V. Wang, G. M. Lanza, *Wiley Interdiscip. Rev. Nanomed. Nanobiotechnol.* **2013**, *5*, 517.
[89] L.-C. Chen, C.-W. Wei, J. S. Souris, S.-H. Cheng, C.-T. Chen, C.-S. Yang, P.-C. Li, L.-W. Lo, *J. Biomed. Opt.* **2010**, *15*, 16010.
[90] K. R. Berry, A. G. Russell, P. a Blake, D. Keith Roper, *Nanotechnology* **2012**, *23*, 375703.
[91] C. R. Crick, J. C. Bear, P. Southern, I. P. Parkin, *J. Mater. Chem. A* **2013**, *1*, 4336.

[92] J. R. Dunklin, G. T. Forcherio, K. R. Berry, D. K. Roper, *ACS Appl. Mater. Interfaces* **2013**, *5*, 8457.
[93] Q. Zhang, J.-J. Xu, Y. Liu, H.-Y. Chen, *Lab Chip* **2008**, *8*, 352.
[94] Y. Shirasaki, G. J. Supran, M. G. Bawendi, V. Bulović, *Nat. Photonics* **2012**, *7*, 13.
[95] E. Z. Zhang, P. C. Beard, In *Proceedings of SPIE Volume 7899*; Oraevsky, A. A.; Wang, L. V., Eds.; 2011; Vol. 7899, p. 78991F–1–6.
[96] J. Zhou, D. A. Khodakov, A. V. Ellis, N. H. Voelcker, *Electrophoresis* **2012**, *33*, 89.
[97] D.-X. Lu, Y.-L. Zhang, D.-D. Han, H. Wang, H. Xia, Q.-D. Chen, H. Ding, H.-B. Sun, *J. Mater. Chem. C* **2015**, *3*, 1751.
[98] T. Scharnweber, R. Truckenmüller, A. M. Schneider, A. Welle, M. Reinhardt, S. Giselbrecht, *Lab Chip* **2011**, *11*, 1368.
[99] J. W. Leem, B. Dudem, J. S. Yu, *RSC Adv.* **2016**, *6*, 79755.
[100] J.-J. Kim, Y. Lee, H. G. Kim, K.-J. Choi, H.-S. Kweon, S. Park, K.-H. Jeong, *Proc. Natl. Acad. Sci.* **2012**, *109*, 18674.
[101] D. J. Lipomi, R. V. Martinez, M. A. Kats, S. H. Kang, P. Kim, J. Aizenberg, F. Capasso, G. M. Whitesides, *Nano Lett.* **2011**, *11*, 632.
[102] Q. Xu, R. Perez-Castillejos, Z. Li, G. M. Whitesides, *Nano Lett.* **2006**, *6*, 2163.
[103] G. Memoli, M. Caleap, M. Asakawa, D. R. Sahoo, B. W. Drinkwater, S. Subramanian, *Nat. Commun.* **2017**, *8*, 14608.
[104] T. J. Hinton, A. Hudson, K. Pusch, A. Lee, A. W. Feinberg, *ACS Biomater. Sci. Eng.* **2016**, *2*, 1781.
[105] M. D. Brown, D. I. Nikitichev, B. E. Treeby, B. T. Cox, *Appl. Phys. Lett.* **2017**, *110*, 94102.
[106] E. J. Alles, S. Noimark, E. Zhang, P. C. Beard, A. E. Desjardins, *Biomed. Opt. Express* **2016**, *7*, 3696.
[107] Y. Sato, K. Mizutani, N. Wakatsuki, T. Nakamura, *Jpn. J. Appl. Phys.* **2008**, *47*, 4354.
[108] J. E. Kennedy, G. R. ter Haar, D. Cranston, *Br. J. Radiol.* **2003**, *76*, 590.
[109] Z. Wu, J. Walish, A. Nolte, L. Zhai, R. E. Cohen, M. F. Rubner, *Adv. Mater.* **2006**, *18*, 2699.
[110] S. W. Lee, S. S. Lee, *Appl. Phys. Lett.* **2007**, *90*, 121129.
[111] M. D. Brown, T. J. Allen, B. T. Cox, B. E. Treeby, In *2014 IEEE International Ultrasonics Symposium*; IEEE, 2014; Vol. 1637, pp. 1037–1040.
[112] R. J. von Gutfeld, D. R. Vigliotti, C. S. Ih, W. R. Scott, *Appl. Phys. Lett.* **1983**, *42*, 1018.
[113] K. Melde, A. G. Mark, T. Qiu, P. Fischer, *Nature* **2016**, *537*, 518.